Research Article

Microbial Mediation in Gypsum Dissolution and Its Role in Evaporitic System Transformation in Northern Chilean Salt Flats

Ivan Orellana[1,2], Cinthya Tebes[1,2], Cecilia Demergasso[2], Óscar Cabestrero Aranda[3,2]

1. Departamento de Ciencias Geológicas, Facultad de Ingeniería y Ciencias Geológicas, Universidad Catolica del Norte, Chile; 2. Centro de Biotecnología Alberto Ruíz, Universidad Catolica del Norte, Chile; 3. Departamento de Mineralogía y Petrología, Facultad de Ciencias Geológicas, Universidad Complutense de Madrid, Spain

The role of microbial consortia in modulating mineralogical processes within polyextreme environments remains underexplored, particularly under controlled laboratory conditions that simulate these environments. This study investigates dissolution and secondary mineral precipitation on synthesized gypsum crystals under abiotic and biotic conditions using microbial mats and natural brines sourced from three Andean salt flats: Llamara, Pajonales, and Gorbea, respectively. Initially, gypsum crystals were synthesized via evaporation of field-collected brines under sterile conditions and then, these crystals were incubated with microbial cultures supplemented by Cyanobacteria medium (BG-11) and sterile brines (controls) under controlled conditions for 90 days. Scanning electron microscopy with energy-dispersive X-ray spectroscopy (SEM-EDS) and epifluorescence microscopy were performed at progressive stages of microbial colonization to monitor gypsum surface alteration, culture growth and microbe-mineral interactions. Results reveal that microbial activity influenced gypsum dissolution in two ways: in some cases, microbial metabolism promoted crystal dissolution, whereas in others, the formation of extracellular polymeric substances (EPS) on top of the crystal surface created diffusion barriers that reduced dissolution. Moreover, EPS matrices facilitated the nucleation of allotriomorphic halite, fibrous Na-Ca sulfates, globular Mg-silicates, dumbbell-shaped calcite (Pajonales-specific), and lenticular Al-K sulfates, while abiotic controls were mineralogically monotonous in comparison. Additionally, microbes showed a tendency to accumulate in the porosities within gypsum crystals and occasionally fill them with EPS and the above-mentioned minerals, although these minerals were also observed on the surface of gypsum crystals. These findings underscore the geomicrobiological complexity of evaporitic systems and support the integration of biotic processes into models of evaporite formation, with implications in astrobiology.

 doi.org/10.32388/ED4EYH

Correspondence: papers@team.qeios.com — Qeios will forward to the authors

1. Introduction

Gypsum (calcium sulfate dihydrate) is a common mineral that is often in contact with or forming part of the substrate that microbes inhabit in arid to hyperarid and even polar environments. As a result, interactions between gypsum and microbes are to be expected, and have been previously reported[1][2] (among many others). Some of these interactions include microbially induced dissolution and precipitation of gypsum, texture alteration, as well as colonization by endolithic bacteria[3][4]. However, the relevance of microbial activity in gypsum dissolution happening in natural settings such as salt flats in hyperarid environments is yet to be assessed.

1.1. Salt flats and previous evaporite formation models

Salt flats are endorheic basins in arid to hyper-arid regions, typically formed through tectonic activity, faulting, and the accumulation of volcanic or alluvial material. These basins usually host lakes, lagoons, drainage systems, or subsurface networks, while surface evaporation produces saline crusts. Their evolution depends largely on water availability: active inflows sustain complex lake systems and ecosystems (e.g., Salar de Atacama), whereas the loss of inputs leads to “salt flat fossilization,” as seen in the Pintados and Bellavista basins, and ultimately to fossil salt flats such as Salar Grande[5].

In northern Chile, salt flats vary according to the geomorphological setting they are inserted in. Chong et al. [5] classified them based on geomorphological setting, a framework followed here to describe the types relevant to this study. In the Central Depression, salt flats typically occur at the distal ends of alluvial fans from the Precordillera and High Andes, with their base level in the depression. Most are fossilizing due to irregular recharge and intensive water use[5]. Salar de Llamara, for example, is receiving low recharge while it accumulates detrital material from the Arcas alluvial fan, an imbalance that may soon fossilize this salt flat. By contrast, High Andean salt flats are the most numerous and youngest, still recharged by water and volcanic/detrital inputs. Some evolve from ephemeral or permanent lakes with fluctuating conditions and their deposits reflect both surface and subsurface inputs with varying compositions even within the same basin. Salar de Pajonales and Salar de Gorbea illustrate this type, located in a volcanic environment and remaining active today.

1.2. Overview of the sampling sites

The three salt flats mentioned in the previous section are localized in the Atacama Desert and its high-altitude Andean margins within Northern Chile, and they were selected for this research (Fig. 1A). They are part of a "Saline Domain" according to Chong et al.[5] reflecting its richness in sulfates, chlorides, nitrates, borates, and iodates, among other salts.

Salar de Llamara (LLA, Fig. 1B) is located in the Pampa del Tamarugal, Tarapacá Region, and is characterized by four shallow lagoons ("puquíos") with surface areas ranging from 1,485 to 4,650 m^2 and depths of 50–100 cm. Surrounding these lagoons are over 400 small ponds, with diameters ranging from sub-metric to decametric scales[6]. The salt flat's deposits, predominantly composed of evaporites, have an estimated thickness of 5–6 meters and include sulfates, chlorides, and minor detrital materials such as silts and clays, forming since at least the Pliocene[7][8][9]. Sediment input originates from the Arcas alluvial fan[10]. Surface waters are nearly neutral, with pH values between 7.0 and 8.3[11][12]. Persistent hyperarid conditions, marked by minimal precipitation, high evaporation rates, elevated temperatures, intense solar radiation, and strong winds, have prevailed since at least the Paleogene[13].

On the other hand, Salar de Pajonales (PAJ, Fig. 1C) is located in the High Andes at the southern edge of the Antofagasta Region, at 3,537 m.a.s.l. and spans 104 km^2, with a catchment area of 2,000 km^2 fed by groundwater inflows. Nearby, the Lomas de la Peña and Quebrado volcanoes, dating from the middle to late Miocene, dominate the landscape[14]. The water of this salt flat is calcium-rich, with Ca^{2+} concentrations exceeding those of SO_4^{2-} and exhibit a pH ranging from slightly acidic (6.5) to slightly basic (8.2)[12]. However, Risacher et al.[15] proposes that the calcium-rich nature of this salar is atypical for its volcanic setting, where carbonate or sulfate-sodium water chemistries would typically prevail. They suggest the Salar de Pajonales may have originated from the reworking of an ancient salt flat, with minimal contribution of new ions from nearby volcanic activity. Common mineral phases found in the salar include halite, gypsum, hexahydrite, ulexite, and calcite.

Lastly, Salar de Gorbea (GOR, Fig. 1D), also located in the High Andes, at an altitude of 3,946 m.a.s.l., spanning 30 km^2 within a catchment of 320 km^2, is surrounded by the Lastarria, Plato de Sopa, and Cerro Bayo volcanoes, part of the Miocene-Holocene volcanic arc[16]. The water of this salt flat is highly acidic, with pH values below 2. Water inputs are primarily from groundwater, driven by the high hydraulic gradient created by the elevation difference between the surrounding volcanoes and the basin, supplemented by small streams descending from the Cerro Bayo complex[17]. Escudero et al.[18] attribute the brine acidity to two main factors: (1) the natural presence of native sulfur in the surrounding area, which then oxidizes to release sulfuric acid

carried by alluvial flows, and (2) intense hydrothermal alteration of the bedrock, which has reduced its buffering capacity. The uppermost layer of the salar is primarily composed of selenitic gypsum, reaching up to 3.5 m in well-preserved zones but typically a few decimeters thick. These layers are intermittently disrupted by brine pools, which have dissolved earlier gypsum deposits. Furthermore, the presence of alunite, along with isotopic signatures of sulfates, serves as evidence of hydrothermal activity during the basin's early development[16]. Common mineral assemblages include halite, thenardite, carnallite, hexahydrite, epsomite, and starkeyite, with trace amounts of kainite, tachyhydrite, Mg-aubertite, and jarosite.

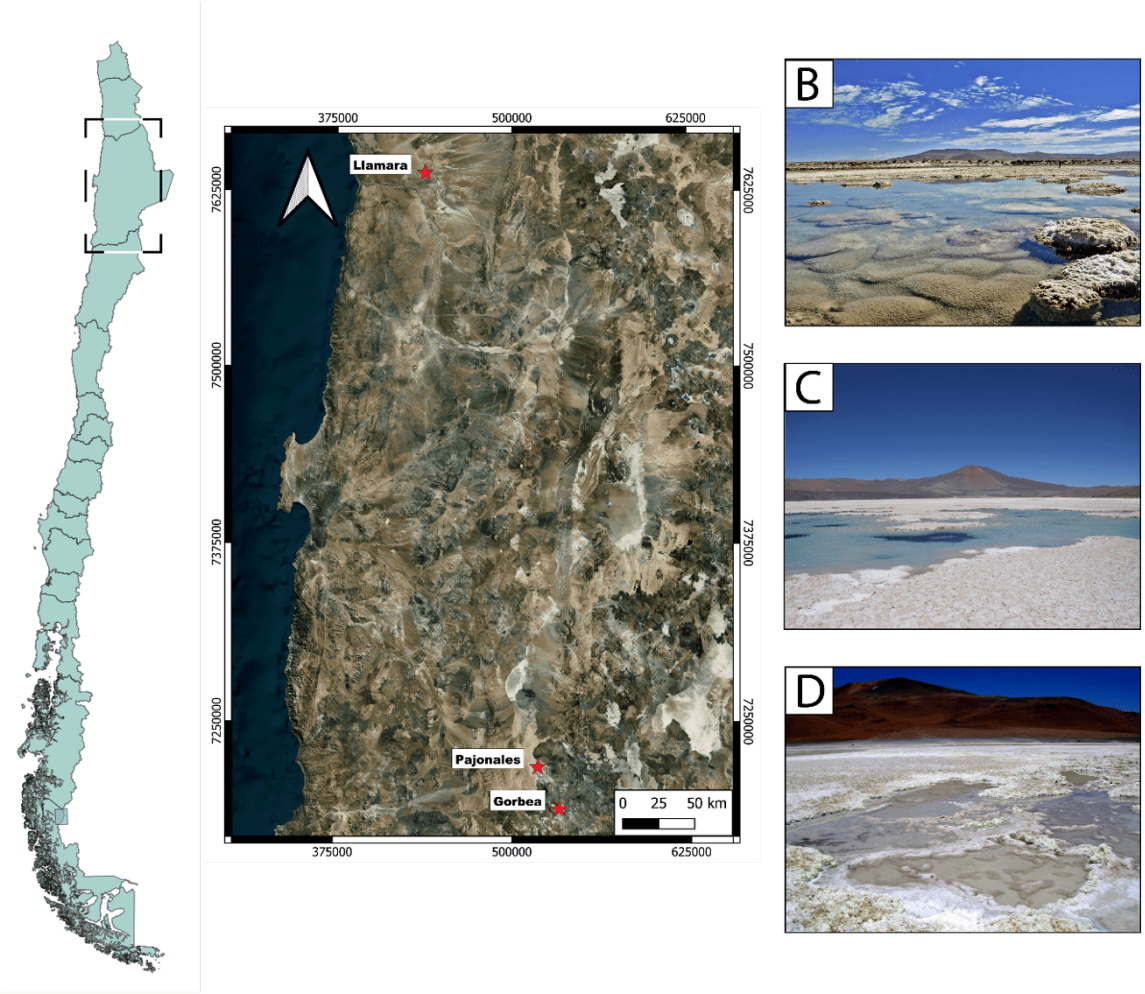

Figure 1. Geolocation of salt flats from which microbial mats were collected. A) Geolocation of the studied salt flats. B) Salar de Llamara. C) Salar de Pajonales. (D) Salar de Gorbea.

1.3. Microbial mineral interactions in evaporitic rocks

The geobiological setting of the above-mentioned salt flats is characterized by a complex interplay between biological activity, water chemistry, and sedimentology resulting in characteristic dynamics. For instance, it has been reported that, in Salar de Llamara, the electrical conductivity (EC) of the water controls the morphology and structure of the lake bottoms, while also modelling bacterial presence and activity because of increasing environmental stress with increasing EC. More specifically, the lower the EC, the more diverse microbial community, and sediments become more carbonate dominated. Conversely, high EC results in a less diverse microbial community and more sulfate-halide dominated sediments[6]. On the other hand, Cabestrero et al.[12] observed that, in presence of microbes, evaporation is not a requirement for evaporitic mineral precipitation in microcosmos from Salar de Pajonales and Salar de Gorbea. They indicated that the collective activity of the microbial consortium can induce mineral precipitation even in undersaturated conditions without evaporation.

In general, mineral precipitation in evaporitic basins has traditionally been associated with ion concentration in brines under evaporative conditions[19][7][20][21][22][23][24][25]. However, newer evidence suggests that microorganisms inhabiting these environments significantly influence mineralization processes This is suggested by different factors such as (1) Distinct textures including dumbbell/rosette, spherulitic, honeycomb arrangements and framboids, among many others[26][27][28][12]; (2) It has also been reported that isotopic signatures from biogenic minerals (specially carbonates) show isotopic disequilibrium with ambient water[29][30]; And (3), the precipitation of mineral phases from undersaturated fluids by locally modulating pH and ion availability through metabolic activity of microorganisms and/or the polar characteristics of the exopolymeric substances they produce, which induces chemical gradients and facilitates nucleation[31].

Under the polyextreme conditions of hyperarid environments, some taxa have adapted to survive or even thrive, which allows them to occupy these ecological niches that are comparatively less competitive. Some of the strategies that they evolved include adaptations to endure high UV radiation, high osmotic pressure, and extreme pH. On the other hand, microorganisms also inhabit sediments and minerals that provide them with a substrate, nutrients, and protection from environmental stress. In endorheic basins, Microorganisms significantly influence sedimentary processes, particularly in evaporitic settings. They form complex microbial mats with morphologies varying from laminar to pustular and bulbous features[11][6]. Moreover, microbial activity from these mats can promote crystal dissolution, which is observed in randomness of ionic detachment, irregular dissolution faces and distorted crystal habits such as abnormally equant crystal shapes which, in the case of gypsum, have only been reported in the presence of organic activity[32][2]. Furthermore, organic compounds such as extracellular polymeric substances (EPS) enhance sediment stabilization, forming

distinctive structures like globular, framboid, alveolar, and radiating arrangements[31][33]. Microbial processes can also drive mineral precipitation[34][26][35] and lithification, with stromatolites representing the most prominent example.

Biomineralization is the precipitation of minerals influenced or controlled by biological activity. Konhauser[36] distinguishes two main pathways: (1) biologically induced biomineralization, where mineral formation arises from an organism's environmental interactions, and (2) biologically controlled biomineralization, where microorganisms actively precipitate minerals or mineraloids as part of metabolism, making them essential for survival. A further mechanism involves ion capture from water by exopolymeric substances (EPS), which create chemical gradients that promote mineral formation.

Notable examples of biomineralization include the precipitation of gypsum mediated by *Synechococcus* sp.[37] and the distinct isotopic fractionation of gypsum in laboratory experiments involving *Acidithiobacillus thiooxidans*[38]. In contrast, carbonate biomineralization has been more extensively studied. For instance, magnesium carbonates have been observed to form through the activity of *Virgibacillus marismortui*, *Marinobacter* sp.[39], and *Desemzia incerta*[40]. Furthermore, calcium carbonate precipitation is commonly associated with EPS produced by mat-forming microbes[35][40][41][42], among many other cases.

Unlike many other minerals in evaporitic deposits, gypsum has been extensively studied from a geological perspective, given its abundance throughout the geological record[4]. However, there are still very few studies focusing on microbe-mineral interactions affecting gypsum, compared to other abundant minerals such as calcite[43]. Consequently, despite the above-mentioned examples, microbial involvement in gypsum mineralization remains poorly understood, and its broader geochemical impact is yet to be fully quantified.

On the other hand, certain microorganisms form endolithic colonies by creating perforations or exploiting fractures in calcium sulfate crystals, though the underlying mechanisms remain uncertain[44][45][46][47][48][49][50]. Organisms forming such colonies tend to migrate millimeters deeper into evaporitic deposits. Wierzchos et al.[51] suggest that cyanobacteria colonies migrate within the gypsum in response to high solar radiation levels. Another defense mechanism against radiation involves the accumulation of metabolites around endolithic colonies. Furthermore, photosynthetic pigments can protect cellular structures, and they change as a response to changes in incident radiation[52].

While numerous studies on microbe-mineral interactions exist, many of them employed synthetic brines, as it was the common approach in the early stages of geomicrobiological studies[53][19][54]. Those settings did not resemble natural water chemistry and, consequently, misrepresented dissolution/precipitation processes happening in natural settings. Furthermore, most previous studies on microbe-mineral interactions focus on

isolated organisms (at the genus or species level), which differ from observations in natural environments where microbiota is diverse. Consequently, there is a limited precedent for monitoring geomicrobiological interactions in natural microbial communities. Recent studies have been more specific in the search for geomicrobiological interactions happening at the microbial community level, but even so is not a faithful representation of the actual conditions present in the field. In this line, the experiments from Cabestrero et al. [12] demonstrated that the activity of microbial assemblages also drives biomineralization processes, hence its study has to include natural-like experimental settings using whole mats and natural brine in order to at least capture the effect of the microbial community as a complex system.

The objective of this study is to enhance our understanding of microbe-mineral interactions through culture experiments in which gypsum crystals were embedded in microbial mats exposed to natural brines, ranging from acidic to hyperalkaline conditions, while excluding the ion-concentrating effects of evaporation. By isolating the crystals, we aim to differentiate textural changes in gypsum caused by microbial activity from those resulting purely from abiotic processes.

2. Methodology

A combination of geological and microbiological techniques was employed to monitor microbial changes in gypsum texture during time-controlled experiments. Whole microbial mat samples, along with their corresponding water collected previously between 2018 and 2020 [12] underwent a selection process prior to experimentation. Texture and morphology alterations in gypsum crystals and geomicrobiological interactions were analyzed using scanning electron microscopy with energy-dispersive X-ray spectroscopy (SEM-EDS). Microbial communities, on the other hand, were observed with optical and fluorescence microscopy. Control experiments with uninoculated gypsum incubations were analyzed in parallel using the same techniques to discern abiotic changes. Additionally, autoclaved brine samples from each salt flat were also observed using optical microscopy to assess mineral presence prior to culture experimentation.

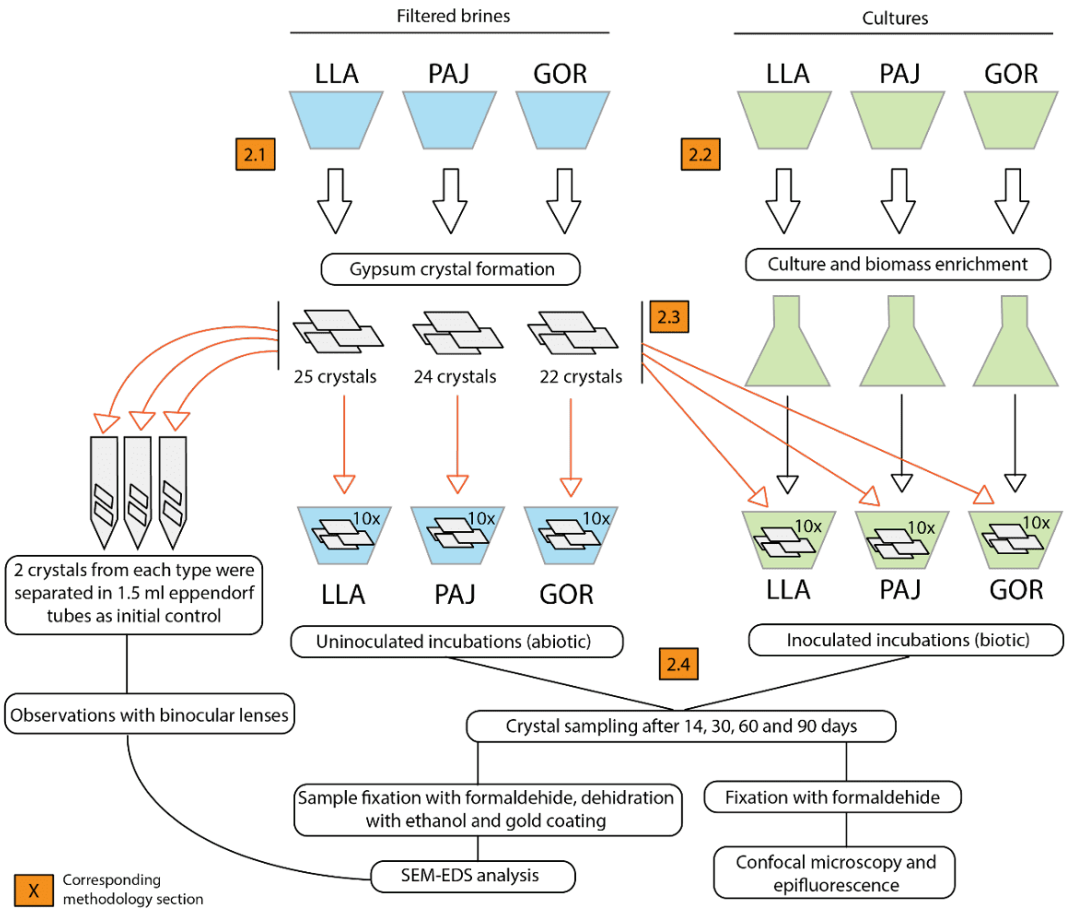

Figure 2. Flowchart illustrating the experimental design and step-by-step process. Step 1 (section 2.1) consisted of selected filtered brines from Salar de Llamará (LLA), Salar de Pajonales (PAJ) and Salar de Gorbea (GOR) were evaporated to obtain gypsum crystals for experimentation. In parallel, BG-11-enriched cultures using intact microbial mat samples with their corresponding water was performed to obtain biomass for inoculation. Then, crystals were placed inside containers with uninoculated and inoculated microcosmos, respectively, while keeping 2 crystals of each morphology intact as control. Crystals were sampled after 14, 30, 60 and 90 days for SEM-EDS and epifluorescence microscopy.

2.1. Water sample selection and gypsum crystal generation

Water samples collected during the campaigns were sequentially filtered through 3 µm and 0.22 µm pore-size filters (Millipore, Burlington, MA, USA) to remove particles and microorganisms. The filtered water was then stored in sterilized plastic containers treated with 80% ethanol until used in the experiments.

Sample selection was based on the gypsum saturation index calculated for brines prior to evaporation using PhreeQC with the Pitzer database[55]. Samples that showed close to supersaturation for gypsum were selected

for the following process. To obtain gypsum crystals for experimentation, 200 mL of selected water samples from the three studied salt flats were filtered through 0.22 µm pore size nitrocellulose filters and placed in open cylindrical glass containers for 2 months. Gypsum crystals were collected periodically as the water evaporated, using plastic coated tweezers and binocular lenses. Gypsum crystal selection involved identifying 10 well-formed, non-twinned crystals measuring 20 mm in length. Crystals were examined using a smartphone camera mounted on a 3D-printed plastic holder for binocular lenses.

2.2. Microbial mat manipulation, culturing and monitoring

Whole microbial mat samples from field campaigns were kept in glass containers with their corresponding water and gypsum substrate at 25°C with 12 hours of light daily in a closed aerobic chamber without agitation [12]. Some microbial mats were well consolidated (PAJ and LLA), with bubbles across the whole mat and even suspended in the water due to the accumulation of gases inside the mat, which caused the detachment. On the other hand, most samples were semi-consolidated and did not present visible layering (i.e. an ideal microbial mat structure) and were partially embedded in EPS (GOR).

To obtain more biomass prior experimentation, 3 samples from LLA, 2 from PAJ and 1 from GOR were selected from Cabestrero et al.[12] cultures. Microbial mats were then subsampled from their original containers using sterile tweezers and the subsamples placed in 1.5 mL Eppendorf tubes. Tubes were taken to a bath sonicator (Elmasonic S 30 H) to remove precipitates, disaggregate the samples, and detach cells that were adhered to mineral surfaces. After sonication, detached and suspended cells were placed in 500 mL sterilized flasks.

To promote cyanobacterial growth and enhance biomass production, the inoculum (10^7 cells/mL) was introduced into 200 mL of culture medium, consisting of BG11 medium (Sigma C3061) at a 1:50 ratio with artificial brine (100 g/L NaCl). The pH was adjusted to 7.5 for PAJ and LLA cultures and 2 for GOR cultures. All procedures were conducted under sterile conditions in a laminar flow chamber (ESCO, Singapore) to prevent contamination. To enhance nutrient diffusion, the flasks were placed on an orbital rotator at 100 rpm inside a closed aerobic light chamber maintained at 24°C. The chamber was equipped with 10 LED lamps (18W, Unilux), providing a total light intensity of >200 $\mu E \cdot m^{-2} \cdot s^{-1}$ in 12-hour light/dark cycles.

Cultures were monitored daily during the first two weeks through cell count, which was performed for each culture to determine whether the medium was optimal for bacterial growth and, thus, biomass production. To perform cell count, 4 µL of water from the mid part of the previously agitated flasks was placed on a Neubauer chamber and observed under an optical microscope (Leica DMLS, Germany). Culture medium replenishment was performed every two weeks to maintain optimal growth of the bacterial communities.

Cyanobacteria and eukaryotic phototrophs were observed through optical microscopy and photosynthetic activity was assessed through fluorescence microscopy (CLSM FV1000, Olympus, Japan) periodically. Morphological identification was performed following Bergey's Manual of systematic bacteorology and Diaz & Maidana[56] for prokaryotes and diatoms, respectively. Identified morphotypes were corroborated with available literature from LLA[11][6], PAJ[57] and GOR[58]. Microorganisms, organic matrix and textures described in Cabestrero et al.[12] were used as a base to describe the structures observed through microscopy techniques. Amoeba identification was based on Salazar et al.[59]. Imagery was obtained using Image Pro-Plus 6.0.0.260 with default settings.

2.3. Experimental setting of culture experiments

Upon 3 months of incubation, a representative subsample of each salt flat was selected, their identifiers were LLA-115, PAJ-40 and GOR-48[12]. The selection was based on which culture had grown the most, while maintaining a healthy green pigmentation. Each flask was bath sonicated and homogenized through agitation. Then, 50 mL of each culture was extracted and placed inside previously autoclaved cylindrical glass containers with a sterile petri dish acting as lid that contained 150 mL of natural brine according to each sampling site. Afterwards, 22 crystals (each) from LLA, PAJ and GOR obtained as described in 2.1 were selected, with 2 of each being stored in Eppendorf tubes filled with paper as control in t=0. Then, 10 crystals of each morphology were placed inside the glass containers with inoculated brine, as well as corresponding abiotic controls (only corresponding autoclaved natural brine without inoculation). All glass containers were then placed inside the light chamber with the same configuration as described in 2.2. Water level was recorded and maintained through replenishment with distilled and autoclaved water to counter any effects of evaporation. Furthermore, cell count, and optical/fluorescent microscopy were performed periodically to assess bacterial growth with the same approach earlier described for the biomass generation process. Additionally, as a response to the unexpected acidophilic fungi contamination of GOR cultures, they were treated with a previously tested Sigma A5955 antibiotic-antimycotic.

2.4. Sample preparation for SEM-EDS analysis

To perform these analyses, 1 gypsum crystal was collected from each container (6 in total) using plastic tools to avoid damaging the samples and then placed in plastic multi-well plates. Between each crystal collection, all tools and surfaces were sterilized with 80% ethanol to avoid cross-contamination of samples. To fix microbial cells present in the samples, 2 mL of 4% paraformaldehyde was added to each well and removed after 24 hours. Then, to dehydrate the samples without causing cell collapse, 20-minute ethanol cycles were performed with 2 mL of 20%, 40%, 60%, 80%, 90%, 95%, 98% and 100% ethanol, the latter being an

overnight cycle. Dilutions were made using the corresponding non-inoculated water of each sample. Ethanol was partially evaporated or extracted from the wells to proceed with the mounting of each crystal on aluminum specimen holders using sterilized plastic tools and carbon tape to fix the samples to the holder. Afterwards, samples were gold-coated using a Desk II Denton Vacuum LLC sputter coater (Moorestown, NJ, USA) to improve image quality on the SEM-EDS. The instrument used to perform the analysis was the Hitachi FE-SEM-EDX, SU5000 (Hitachi, Tokyo, Japan) equipped with energy dispersive X-ray spectroscopy to obtain elemental composition of samples, along with spectral mapping. These analyses were repeated after 14, 30, 60 and 90 days to analyze textural changes on the gypsum crystals.

3. Results

The interactions between gypsum crystals and microbes revealed intriguing processes of dissolution and precipitation that help elucidate the interplay between microbial activity and mineral dynamics. This analysis highlighted the unique morphological and compositional characteristics of gypsum crystals from Salar de Llamara (LLA), Salar de Pajonales (PAJ), and Salar de Gorbea (GOR), along with the temporal changes observed during incubation. By comparing experimental and control samples, significant differences in abiotic and biotic dissolution emerged, along with the development of extracellular polymeric substance (EPS) layers and the precipitation of secondary mineral phases.

3.1. Brine geochemistry and gypsum initial conditions

For all selected brine samples, gypsum saturation index indicated near balance. For instance, LLA showed a SI value of 0, while PAJ showed -0.01, and GOR 0.14. This was also corroborated by the fact that evaporating the brines, so they lost about 30% of their volume, gypsum started precipitating. Saturation indexes for other common evaporitic mineral phases were calculated (Table 1).

The gypsum crystals that grew from evaporating the brine samples exhibited strikingly different initial morphologies depending on their origin. At LLA, the crystals were mostly prismatic, slender forms reaching lengths of up to 3 mm (Fig. 3A). In contrast, those from PAJ were considerably larger—up to 3 cm—and displayed a well-developed tabular habit (Fig. 3B). These often showed fishtail twinning and secondary overgrowths, expressed as delicate tabular crystals roughly 50 µm wide that adhered to the main surfaces. GOR samples, on the other hand, were composed of fine acicular crystals extending to about 4 mm in length (Fig. 3C). Under optical and scanning electron microscopy (Fig. 3A–F), all gypsum crystals appeared relatively smooth; yet closer inspection revealed subtle differences. GOR crystals, in particular, exhibited more irregular surfaces, showing early signs of dissolution along their edges and sparse aggregates of secondary minerals

atop (Fig. 3F). Together, these textural and morphological contrasts likely influenced the distinct evolutionary trends observed between the experimental runs and the abiotic controls.

Sample ID		**P117**	**M2.4**	**GOR-4**
Salt flat		**Llamara**	**Pajonales**	**Gorbea**
Parameter	**Unit**			
Date	**MM/DD/YY**	**9/14/2020**	**10/22/2019**	**3/12/2020**
Na^+	mg/L	6330	41538	9970
Mg^{2+}	mg/L	130	2776	4110
Ca^{2+}	mg/L	780	7260	764
K^+	mg/L	176	1720	762
Mn^{2+}	mg/L	0	0	73
Cl^-	mg/L	7720	86240	21100
$SO4^{2-}$	mg/L	5680	1970	20550
Fe^{2+}	mg/L	0.3	0.8	66.6
Alkalinity	mg/L HCO_3^-	300	457	0
Salinity	%	2.9	15.2	6.0
EC	µS/cm	27140	169700	61300
Temperatue	ºC	21.1	10.2	18.0
pH		8.3	7.4	1.9
Gypsum SI	log Q/K	0.00	-0.01	0.14
Glauberite SI	log Q/K	-2.95	-2.42	-2.19
Halite SI	log Q/K	-3.26	-1.29	-2.57
Thenardite SI	log Q/K	-3.40	-2.90	-2.77
Calcite SI	log Q/K	1.08	1.68	-

Table 1. Geochemistry of water samples used for culturing and experimentation.

doi.org/10.32388/ED4EYH

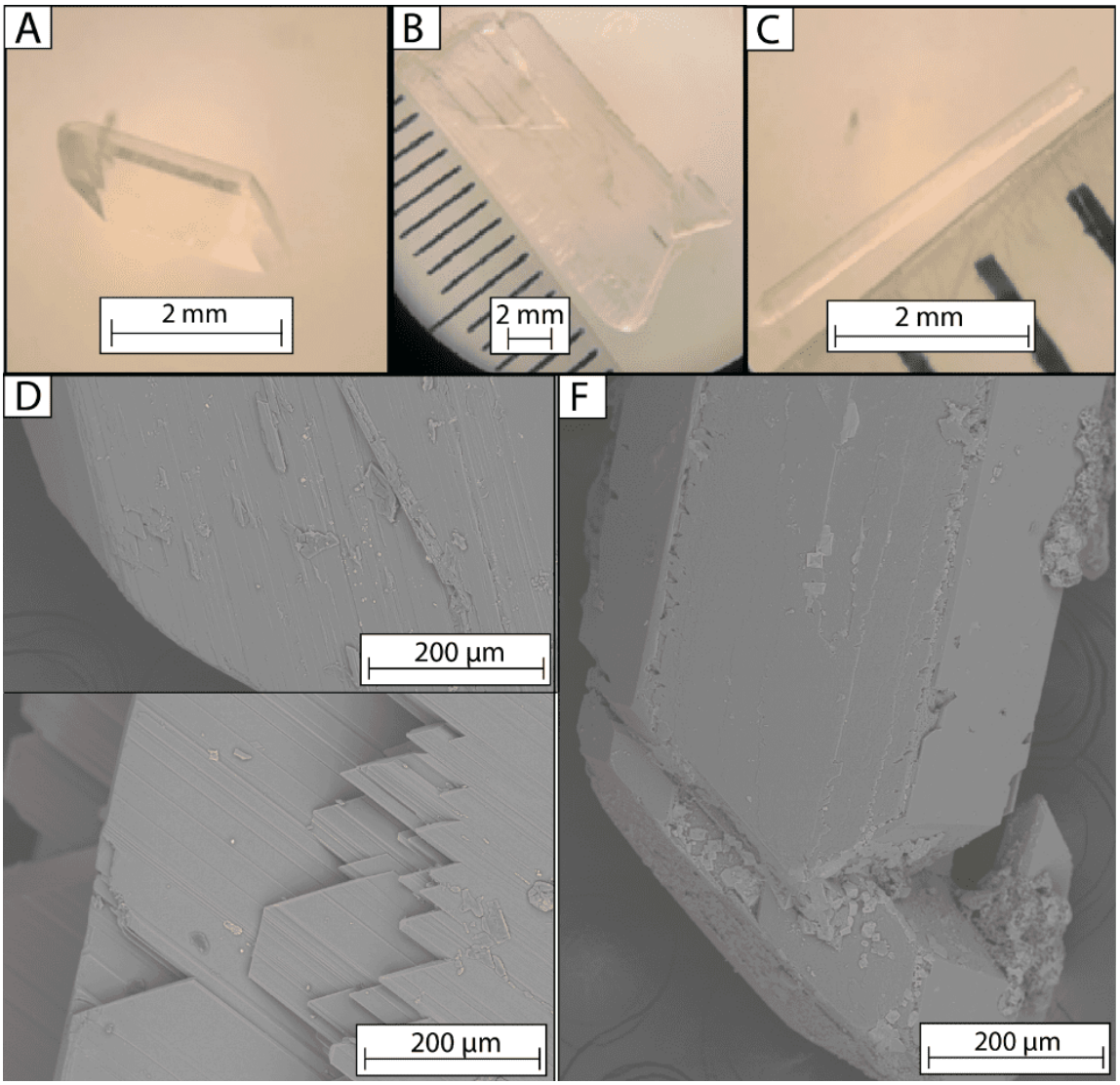

Figure 3. Gypsum crystal morphologies observed under binocular lenses (A-C) and model crystal microphotographs captured via SEM. (A) Well-developed prismatic LLA crystal with no signs of dissolution. (B) Tabular PAJ crystal displaying cleavage planes and no dissolution. (C) Acicular GOR twinned crystal and occasional mineral aggregates atop.

3.2. Culture evolution over time

Cultures exhibited significant changes in coloration, turbidity, and bacterial abundance over the course of the experiment (Table 2). The following paragraphs detail these findings, integrating visual observations, microbial dynamics, and mineral transformations.

Bacterial growth curves revealed similar trends between LLA and PAJ cultures, while GOR displayed a notably different evolution. In particular, LLA cultures were initially transparent with minimal turbidity, but they

acquired green hue as they were dominated by photosynthetic microorganisms after a week. Moreover, LLA cultures experienced exponential growth of photosynthetic cells between days 14 and 60, while maintaining green coloration, after which a short plateau and subsequent decline in cell count was observed (Fig. 4A). Similarly, PAJ cultures started transparent but acquired slightly moss green hue by 14 days, along with increased turbidity until 60 days, later shifting to a pale orange hue at 90 days. This color change is coherent with the photosynthetic pigment degradation observed under microscope, as well as the increase in abundance of non-photosynthetic cells (Fig. 4B). In contrast, GOR cultures evolved differently as PAJ and LLA cultures due to grown of acidophilic fungi, which gave cultures moderate turbidity from the start of the experiment (sterile controls were not affected). These cultures acquired a pale green hue after antifungal treatment, accompanied by the recovery of coccoid cyanobacteria up until the end of experimentation, as suggested by the absence of a bacterial death phase in the 3-month span of the experiment (Fig. 4C).

Culture	Time [days]	Photosinthetic cells [cell/mL]	Active photosinthetic cells [cell/mL]	Inactive photosinthetic cells [cell/mL]	Non-fluorescent cells [cell/mL]	Living[52]	Color	Turbidity	
LLA	0	6.20.E+05	6.20.E+05	0.00.E+00	0.00.E+00	100%	Transparent	*	
	14	4.33.E+06	3.66.E+06	6.72.E+05	1.24.E+07	84%	Pale green	*	
		30	4.37.E+06	1.17.E+06	3.20.E+06	1.28.E+07	27%	Apple green	**
		60	6.78.E+07	1.94.E+07	4.84.E+07	1.94.E+07	29%	Apple green	***
	90	2.71.E+06	6.78.E+05	2.03.E+06	0.00.E+00	25%	Apple green	**	
PAJ	0	7.31.E+06	6.56.E+06	7.53.E+05	0.00.E+00	90%	Transparent	*	
	14	5.87.E+06	2.69.E+06	3.18.E+06	3.41.E+06	46%	Green	**	
		30	9.01.E+06	6.27.E+06	2.74.E+06	3.80.E+06	70%	Orange	**
		60	2.42.E+07	2.11.E+07	3.15.E+06	6.41.E+07	87%	Brown	***
	90	2.42.E+05	0.00.E+00	2.42.E+05	5.08.E+06	0%	Pale orange	**	
GOR	0	1.00E+07	1.00E+07	0.00E+00	n.a.	100%	White	**	
	14	4.00E+05	4.00E+05	0.00E+00	n.a.	100%	Light green	***	
		30	3.00E+06	7.00E+05	2.00E+06	n.a.	23%	Moss green	**
	90	4.00E+07	2.00E+07	2.00E+07	n.a.	50%	Pale green	**	

Table 2. Summary of evolution of cultures over time. Turbidity is indicated as * (low), ** (medium) and *** (high).

doi.org/10.32388/ED4EYH

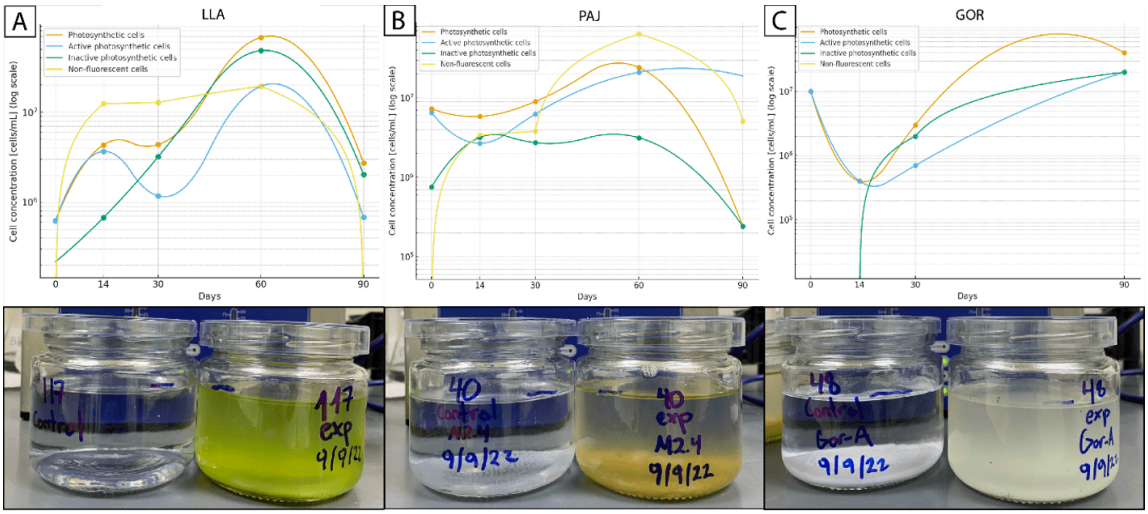

Figure 4. Experimental setup for gypsum dissolution under microbial growth in BG-11 medium with sterile brines, incubated at 24°C with constant agitation of 100 rpm in a closed aerobic light chamber, with a total light intensity of >200 $\mu E \cdot m^{-2} \cdot s^{-1}$ in 12-hour light/dark cycles. Specific growth curve for LLA (A), PAJ (B), and GOR (C) cultures. Note: below each curve there are their corresponding control (left) and experiment (right) glass containers after 90 days of experimentation. As exhibited by the absence of color and reaffirmation through microscopy, controls did not show microbial growth nor presence after 90 days.

On the other hand, while all cultures exhibited microbial growth, each different culture showed distinct predominant cellular morphotypes under the optical microscope. In each case, different relationships between microorganisms and crystals were also observed under SEM. For instance, cultures from Salar de Llamara were dominated by 10 µm double flagellated oval algae resembling as *Dunalliella*, and fusiform diatoms up to 50 µm (Fig. 5A), the latter being unique to LLA and becoming less present by the end of experimentation. Furthermore, SEM observations showed that bacterial growth in LLA was followed by the embedding of small crystals and cells in a growing EPS matrix (Fig. 5B). By the end of experimentation, the EPS layer had thickened and covered most of the gypsum surface (Fig. 5C), which is coherent with the agglutination observed under optical microscopy. Additionally, EPS-embedded coccoid cells were adhered to the gypsum crystal surface.

On the other hand, PAJ cultures were dominated by bacillar diploids up to 20 µm in size that exhibited red fluorescence (Fig. 5D). Additionally, and distinctively for PAJ, 150 µm spiral cyanobacteria were observed after 14 days of incubation, some of which had degraded pigments (Fig. 5E). Like LLA, PAJ crystals were partially covered by EPS after the first 30 days of experimentation, and it embedded unicellular and diploid cells resembling of Gloeocapsa, newly formed sulfate crystals, and 5 µm dumbbell-shaped calcite on top of the

gypsum (Fig. 5F). In addition, 10 µm globular organic structures were found adhered to the gypsum surface (Fig. 5G).

In parallel, up to 60 µm long conidia and conidiophores overshadowed the scarce phototrophs in GOR sample, which displayed fluorescence (Fig. 5H). After antimycotic treatment, fungal presence declined and both algae and procaryotes slowly recovered (Fig. 5I). Furthermore, and following the trend observed under optical microscopy, GOR crystals were covered by EPS at a slower rate after antimycotic treatment. By the end of the experiment, GOR crystals were partially covered in EPS-embedded cells and crystals, mainly those of lenticular morphology (Fig. 5J).

doi.org/10.32388/ED4EYH

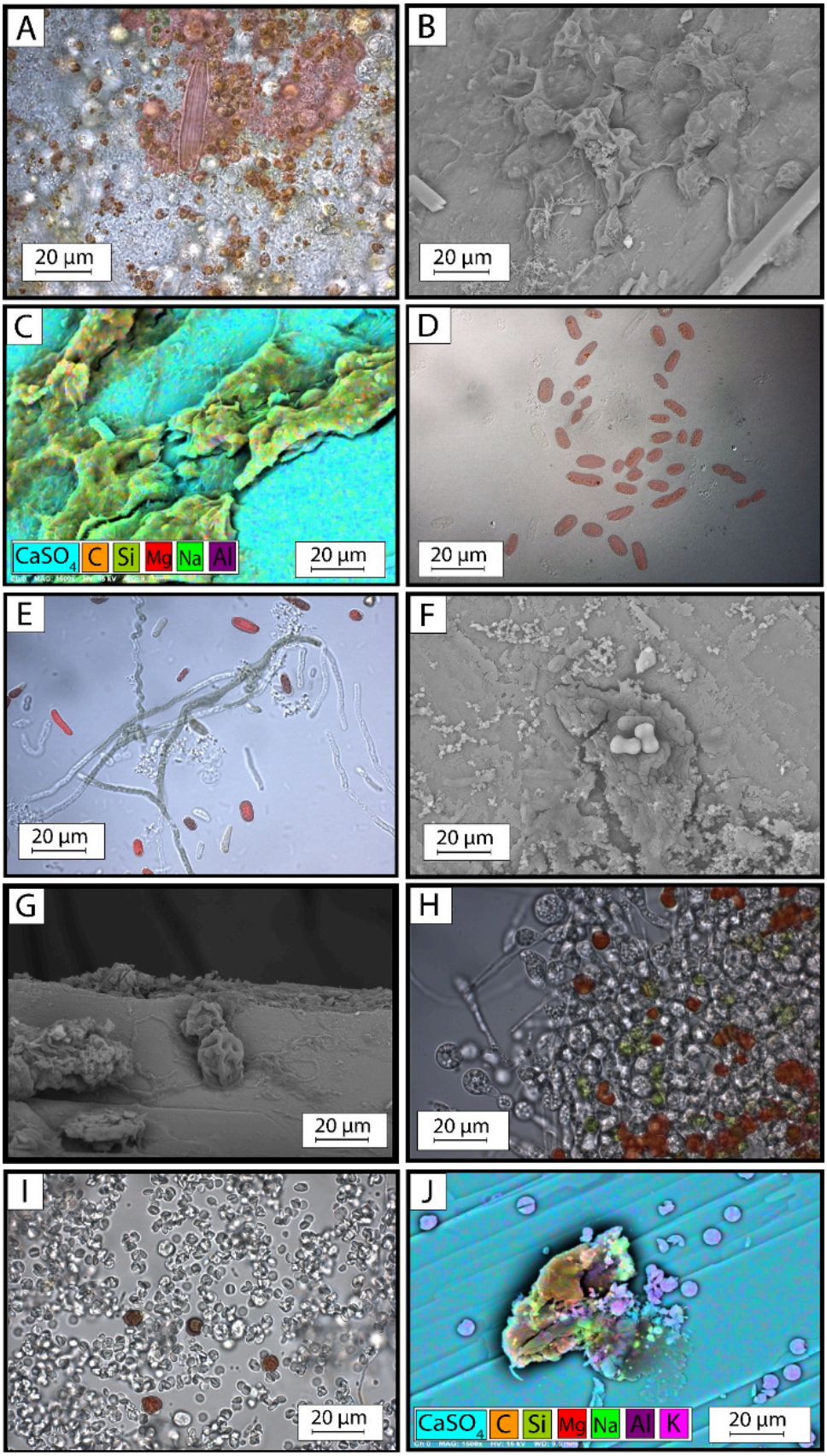

doi.org/10.32388/ED4EYH

Figure 5. Images of cell morphotypes and crystals observed in LLA, PAJ, and GOR cultures, combining brightfield and epifluorescence microscopy (A, D, E, H, and I) with SEM-EDS micrographs (B, C, F, G, and J). (A) In LLA cultures, *Dunaliella*-like algae and fusiform diatoms highlighted with red auto-fluorescent. (B-C) LLA crystals partially covered by a thick EPS layer embedding crystals and cells, also forming globular structures. (D) Bacillar diploids with red auto-fluorescence in PAJ cultures. (E) Spiral and filamentous cyanobacteria showing degraded pigments in PAJ at 14 days of incubation. (F) PAJ tabular crystals covered globular aggregates within an EPS matrix with occasional dumbbell calcite. (G) Globular organic structures on PAJ gypsum crystal surface. (H) Conidia (yellow) and conidiophores (red) in the fungi-contaminated GOR outnumbering green algae (white) prior to antifungal treatment. (I) 2 to 5 µm lenticular crystals and 5 to 10 µm fluorescent algae in GOR after antimycotic treatment. (J) EPS embedded lenticular crystals and cells on top of the unaltered GOR crystals.

3.3. Resulting conditions

Under experimental conditions, the interplay between gypsum dissolution and secondary mineral precipitation varied depending on initial microbial mat texture, gypsum crystal morphology (both of which depend on source lake), and the environmental context, that is, in the presence or absence of microorganisms.

In abiotic experiments, gypsum crystals showed textural alterations characterized by apparent greater porosity over time, as compared to inoculated samples. These porosities had commonly jagged or abrupt edges throughout all samples, while their occurrence and morphology were distinct for each sample group. LLA crystals, for instance, started with a smooth surface but developed pronounced cleavage planes, along which dissolution happens faster (Fig. 6A). As time progressed, fibrous Na-Ca sulfates covered most of the crystal surface (Fig. 6B). Later on, crystal surface became flaky with minerals filling in the occasional elongated and circular porosities. PAJ crystals, on the other hand, were smooth at the beginning, but quickly developed a flaky surface with increasing porosity of elongated, circular and irregular morphologies. These porosities were not filled with newly formed minerals, although occasional subhedral to euhedral halite and gypsum crystals were present (Fig. 6C-D). GOR crystals, distinctively, started with an already irregular surface that was partially covered by mineral aggregates. As time progressed, occasional partially filled porosities along planes and irregular fractures were observed (Fig. 6E-F) (Table 3).

	Time [days]	Gypsum suface	Porosity			Observed minerals
			Max. Mayor axis size [µm]	Frequency [N/10000µm2]	Porosity filling	
LLA	0	Smooth	-	-	-	-
	14	Smooth	-	>2	No	Gypsum, lenticular Na-Ca sulfate
	30	Porous/dissolution along planes	20	>6	No	No change
	60	Fractures/dissolution along planes	50	>10	No	No change
	90	Fractures and dissolution along planes/Mineral cover	50	>10	Fibrous Na-Ca sulfates	No change
PAJ	0	Smooth	-	-	-	-
	14	Porous/flaky	155	>6	No	Gypsum
	30	Porous/flaky	225	>9	No	Euhedral halite
	60	Porous/flaky	210	>10	No	No change
	90	Porous/flaky	335	>10	No	Mg-Si globules
GOR	0	Irregular edges and precipitates	-	-	-	-
	14	Irregular edges and precipitates	-	-	-	Gypsum, lenticular K-Al sulfate
	30	Irregular edges and precipitates	-	-	No	No change
	60	Irregular edges and precipitates	-	-	Lenticular crystal aggregates	No change

doi.org/10.32388/ED4EYH

	Time [days]	Gypsum suface	Porosity			Observed minerals
			Max. Mayor axis size [µm]	Frequency [N/10000µm2]	Porosity filling	
	90	Irregular edges and precipitates	135	>4	Lenticular crystal aggregates	No change

Table 3. Summary of control gypsum surface characteristics, porosity, and mineral precipitation over time (NM: not measurable).

doi.org/10.32388/ED4EYH

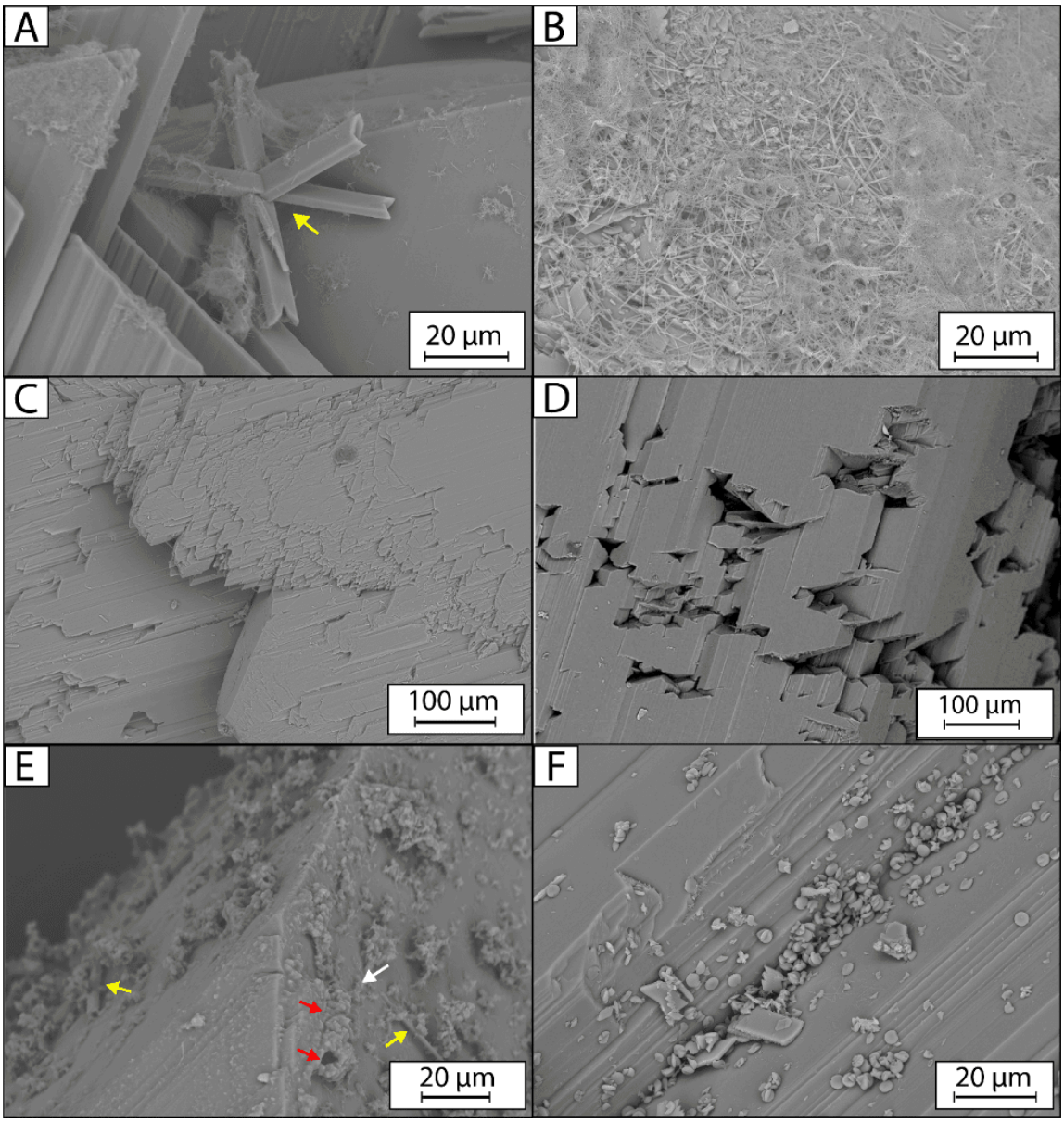

Figure 6. SEM microphotographs of LLA (A-B), PAJ (B-C) and GOR (E-F) control gypsum crystals. (A) Fishtail twinning, distinct cleavage planes and radial gypsum with fibrous aggregates atop (yellow arrow). (B) EPS-embedded fibrous Na-Ca sulfate covering most of the gypsum surface. (C) Flaky and porous gypsum surface with exposed cleavage planes. (D) Heavily dissolved gypsum surface, with several hundred micrometer fractures and cavities preferably along cleavage planes. (E) Newly formed gypsum (yellow arrows), fibrous Na-Ca sulfate (white arrow) and scarce globular precipitates (red arrows) on top of the gypsum. (F) Twinned lenticular crystals filling fractures in the gypsum, as well as newly formed prismatic gypsum.

In the presence of microorganisms, by day 14, an EPS film had covered the surfaces of all crystal types, most prominently on LLA and PAJ crystals (Fig. 7). This biofilm progressively thickened and served as a nucleation

surface for secondary mineral precipitation. In LLA samples, prismatic Na-Ca sulfate crystals (2–5 µm) formed preferably associated with EPS as early as 14 days from the start of the experiment (Fig. 7A). These crystals increased in quantity throughout the experiment, as they were embedded in the EPS matrix, which by day 90 had contracted and formed globular structures (Fig. 7B-C). In PAJ samples, on the other hand, dissolution features were present from day 14 and became prominent by day 30, with halite and Mg-silicates forming preferably on EPS within dissolution cavities (Fig. 7D). By day 60, isolated calcite crystals with dumbbell morphologies (3–6 µm) had appeared, as well as more Mg-silicates on top of the extending EPS layer (Fig. 7E). By the end of the experiment, lenticular K-Al sulfates were also present (Fig. 7F). In GOR samples, secondary mineral formation was limited but included twinned lenticular aggregates of K-Al sulfates with traces of organic material from day 14 (Fig. 7G), which increased in quantity towards day 60 (Fig. 7H). By the end of the experiment (day 90), GOR crystal surfaces were heavily altered, and the lenticular aggregates were apparently completely covered by EPS and newly formed gypsum (Fig. 7I) (Table 4).

When comparing dissolution and precipitation rates among abiotic and biotic cultures, notable differences and similarities arise. For instance, LLA crystals in both cases showed scarce abiotic dissolution, while Na-Ca sulfate precipitation was notably faster in experimental samples, as seen in early observations (Fig. 6A and 7A). In the case of PAJ samples, crystals without microbes displayed higher porosity and no filling, while experiment crystal porosities were filled by EPS and other minerals (Fig. 6D and Fig. 7F). On the other hand, GOR crystals evolved similarly in both abiotic and biotic cultures, with gypsum dissolution apparently starting later during experimentation. The main difference between the samples was the rate at which the lenticular aggregates accumulated on top of the gypsum surface, with experimental samples displaying a faster rate.

	Time [days]	Gypsum suface	Porosity			Newly observed minerals
			Max. Mayor axis size [µm]	Frequency [N/10000µm2]	Porosity filling	
LLA	0	Smooth	-	-	-	-
	14	Alveolar organic cover	-	NM	EPS-embedded fibrous Na-Ca sulfate crystals	Gypsum, fibrous Na-Ca sulfate
	30	Alveolar organic cover	20	>4	EPS-embedded 67 µm Gp crystals	No change
	60	Alveolar organic cover	50	>4	EPS-embedded Gp, Na-Ca sulfates and Mg-Si globules	Mg-Si globules
	90	Alveolar organic/mineral cover	NM	>1	EPS-embedded Gp, Na-Ca sulfates and Mg-Si globules	No change
PAJ	0	Smooth	-	-	-	-
	14	Smooth	NM	>1	Worm-like halite and 2 µm Mg-Si globules	Gypsum, allotriomorfic halite, Mg-Si globules
	30	Organic cover	115	>2	EPS-embedded 2 µm Mg-Si globules	Dumbbell-shaped calcite
	60	Organic cover	10	>1	Alveolar EPS-embedded 2 µm Mg-Si globules and Gp crystals	No change
	90	Organic cover	40	>1	Alveolar EPS-embedded 2 µm Mg-Si globules and Gp crystals	Lenticular K-Al sulfate
GOR	0	Irregular edges and precipitates	-	-	-	-
	14	Irregular edges and precipitates	-	-	-	Gypsum, lenticular K-Al sulfate

	Time [days]	Gypsum suface	Porosity			Newly observed minerals
			Max. Mayor axis size [µm]	Frequency [N/10000µm2]	Porosity filling	
	30	Irregular edges and precipitates	80	>6	Lenticular crystal aggregates	No change
	60	Organic/mineral cover	60	>2	Lenticular crystal aggregates and Na-Ca sulfates	Fibrous Na-Ca sulfate
	90	Organic/mineral cover	NM	>1	Lenticular crystal aggregates and Na-Ca sulfates embedded in EPS	No change

Table 4. Summary of experiment gypsum surface characteristics, porosity, and mineral precipitation over time (NM: not measurable).

doi.org/10.32388/ED4EYH

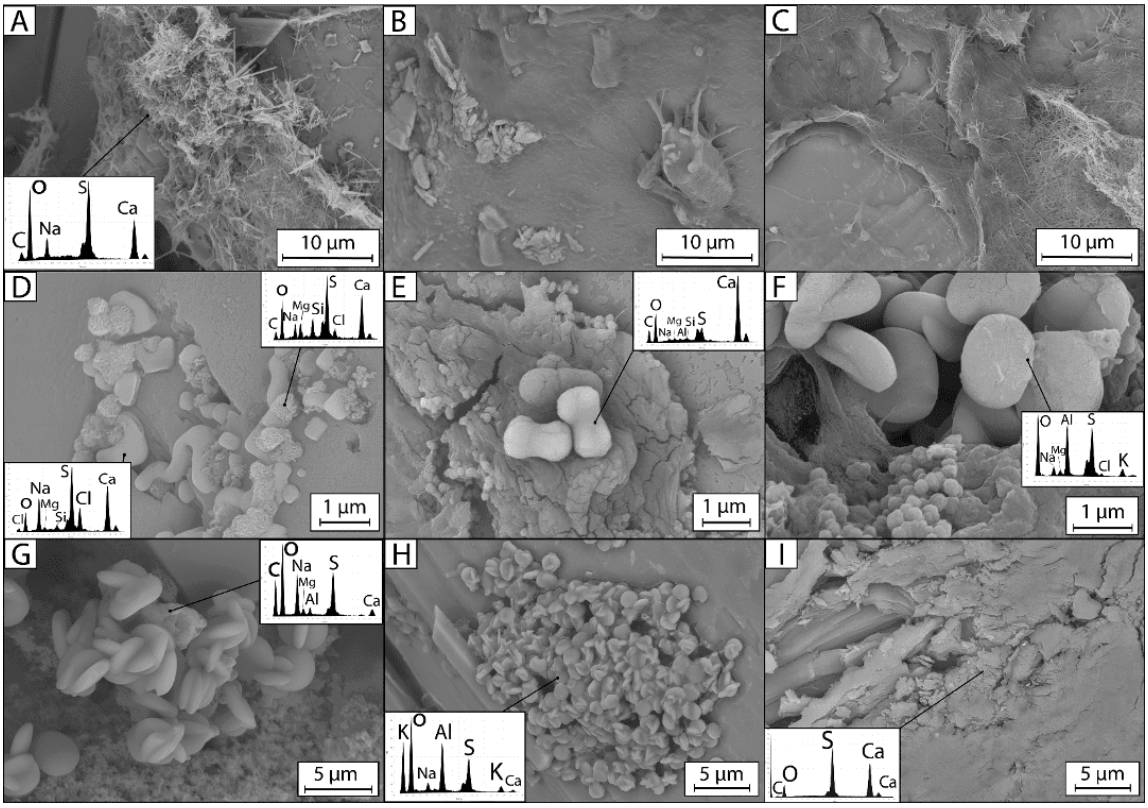

Figure 7. SEM microphotographs of LLA (A-C), PAJ (D-F) and GOR (G-I) experiment gypsum crystals at 0 (first column), 35 (second column) and 90 days (third column). (A) Fibrous Na-Ca sulfate within and on top the alveolar EPS partially covering the LLA gypsum surface. (B) Thicker EPS layer embedding newly formed gypsum crystals. (C) Alveolar EPS embedding cells, fibrous Na-Ca sulfates and gypsum, and forming globular structures. (D) Mg-Silicate rugose globules and allotriomorphic halite filling porosities in PAJ gypsum. (E) Dumbbell-shaped calcite along with Mg-Si globules on top of the EPS. (F) Alveolar EPS-covered gypsum with Mg-Si globules and twinned lenticular K-Al sulfate on top. (G) Twinned lenticular K-Al sulfates with smooth surfaces with traces of C on top of a GOR gypsum crystal. (H) Lenticular crystal aggregates with jagged edges partially covering the gypsum surface, with scarce newly formed gypsum crystals. (I) Heavily altered gypsum surface with traces of carbon indicative of organic matter.

4. Discussion

This study provides new insights into the role of microorganisms in gypsum dissolution under saline lake conditions characterized by variable pH and salinity. The experiments demonstrate that dissolution dynamics differ between biotic and abiotic systems, indicating that microbial activity exerts a measurable influence on mineral–water interactions. Such influence affects dissolution rates, surface morphologies, and secondary mineral formation, revealing that these processes are not exclusively controlled by abiotic factors. These

results align with previous observations of microbially mediated gypsum alteration and replacement[33][60][61]. Overall, the findings refine traditional abiotic models of evaporite formation by integrating biochemical interactions into the framework governing the evolution of Andean salt flat deposits.

4.1. Gypsum Dissolution: Transformations Driven by Endolithic Microbial Activity

Both control and microorganism-inoculated gypsum crystals showed early evidence of dissolution within the first month of exposure. These features included cavities, fractures, and irregular dissolution along crystal edges. However, clear differences were observed between treatments. Cavities in the microbially exposed crystals had smooth and rounded walls, whereas those in the controls were jagged and angular. Dissolution in the control samples likely occurred because the brine used in the experiments was undersaturated with respect to gypsum. Since the crystals had initially precipitated by evaporation, reintroducing them into non-evaporated brine favored partial dissolution.

The morphology of the smooth cavities in experiment samples resembles features previously attributed to endolithic colonization. Rothschild et al.[62] first described microbial boring in gypsum, which Sanz-Montero et al.[63] and Wierzchos et al.[48][49] later associated with endolithic activity capable of penetrating mineral substrates.

Over time, gypsum dissolution proceeded more slowly in the presence of microorganisms. The abundance and size of pores were lower in experiment samples compared to controls, indicating that microbial colonization affected the dissolution rate. The near-zero saturation index of the brine explains dissolution in controls, while the microbial biofilm modified this process in the inoculated systems. In these, pores were partially filled or covered by extracellular polymeric substances (EPS) and mineral precipitates. This observation is consistent with Venturi et al.[60], who reported slower gypsum dissolution in EPS-coated crystals due to reduced ion mobility across the mineral–water interface. In the present study, EPS accumulation increased through time and nearly covered the surface of LLA and PAJ crystals after two months, which coincided with reduced porosity (Table 1).

In LLA samples, pore abundance and size were similar between controls and experiments. This suggests that microbial activity may also promote dissolution under certain conditions, for example through endolithic boring or metabolism that destabilizes the crystal structure. Control samples followed a more linear trend. LLA and GOR controls remained relatively intact, while PAJ controls developed larger and more numerous cavities. This pattern highlights the role of microbial metabolism in modifying gypsum stability. Sulfate-reducing bacteria can use sulfate from gypsum as an electron acceptor, leading to mineral dissolution, while As(V)-reducing bacteria, common in PAJ and GOR waters, can also promote gypsum instability[64]. In addition,

degradation of the EPS matrix can locally increase pH and lower the gypsum saturation index, favoring its replacement by carbonates, as reported by Thompson and Ferris[37], Cody and Cody[32] (1990), and Vogel et al.[2] (2010).

Despite these potential dissolution mechanisms, the lower porosity in experiment samples indicates an overall slower rate of gypsum dissolution in the presence of microorganisms. This may reflect the relatively short duration of the experiment, which limited EPS degradation and associated alkalinization. Another possibility is that pores were present but covered by EPS and therefore less visible.

Gypsum dissolution was also observed during halite precipitation, both in the preparation of synthetic crystals and in the experimental microcosms. Previous studies[65][66] showed that gypsum solubility increases with NaCl concentration, reaching a maximum near 3 M. The localized precipitation of halite on gypsum surfaces therefore likely enhanced gypsum dissolution, an effect most evident in PAJ samples.

4.2. Microbial Community Variations and Gypsum Colonization

The experimental setup used BG11 medium to favor photosynthetic microorganisms and increase biomass prior to gypsum exposure. As a result, the microbial diversity observed in these cultures does not reflect the composition typically reported for natural salt flats[67][58][68][69]. Laboratory-enriched communities are known to display lower diversity than their natural counterparts[70]. Although natural brine samples were employed in this study, other environmental variables such as wind, solar radiation, and sediment dynamics could not be reproduced under laboratory conditions.

In LLA and PAJ cultures, microbial growth followed a typical pattern, with photosynthetic cell abundance peaking after 60 days. The number of microorganisms and the amount of extracellular polymeric substances (EPS) attached to the gypsum surfaces increased progressively during this period. This trend is likely related to the dominance of cyanobacteria, favored by the BG11 enrichment. Cyanobacteria are known to bore into gypsum crystals, forming endolithic colonies[62], and are among the most efficient producers of EPS within photosynthetic mats, particularly under environmental stress[71][72]. The activity of these microorganisms likely contributed to the progressive thickening of the EPS layer observed in experimental samples.

In contrast, GOR cultures showed a distinct evolution, as revealed by SEM observations. This difference may result from the antifungal treatment applied to these samples, which contained small amounts of antibiotics that also affected bacterial populations and possibly reduced EPS production. After 60 days of incubation, however, the abundance of prokaryotes in GOR increased noticeably, suggesting slower microbial growth compared to the other systems. This delayed development could reflect either a response to the antifungal treatment, or an intrinsic characteristic of microbial communities adapted to the polyextreme environment of

Salar de Gorbea[18]. Previous studies have also documented slow-growing bacterial taxa in this site, consistent with the environmental constraints observed there[73].

As mentioned in the previous section, gypsum colonization by microbes was observed extensively specially in round-edged cavities in the crystals (Fig. 7D-F). This has been reported by many authors attributing this colonization pattern to the availability of water in gypsum, which serves as a microbiological niche in dry conditions due to its ability to retain humidity[1][74][51]. For instance, relative humidity in the gypsum crust at Salar de Pajonales fluctuates between 13-36% reaching higher peaks during rare and brief rain events. This has also been reported at Llanos de la Paciencia[1], Lomas de Tilocar and Cordón de Lila[74][51], and in the southernmost part of the Tarapacá Region[46]. Considering humidity retention and incident UV radiation filtering by gypsum, these reports provide proof that gypsum provides the necessary conditions for photosynthetical microorganisms to grow and thrive.

4.3. Mineral paragenesis in Experimental Precipitation

In general, mineral precipitates that nucleated in control samples were only found on the surface of the gypsum crystal, whereas in presence of microorganisms, a more diverse array of minerals nucleated preferably in EPS-filled porosities and EPS-coated gypsum surfaces. This suggests that microbial activity in experimental samples induces chemical properties different enough from their inorganic counterparts that result in this difference in the mineral assemblages precipitated in both cases. Moreover, nucleation was not observed in the water itself, further supporting the idea that microbial colonization of gypsum drives these nucleation processes in undersaturated conditions (Table 1). Overall, these results confirm what was observed in previous studies that attended microbial consortia mediation in mineral precipitation.

Newly formed Ca- and Na–Ca-sulfate minerals displayed textural and structural features indicative of biochemical influence on their formation. Similar characteristics have been reported for gypsum and other minerals affected by microbial activity, including distinctive crystal morphologies and the development of crystal defects[37][4][75][76].

Overall, the observed mineral assemblages suggest that microbial processes favored earlier precipitation of secondary mineral phases compared to abiotic controls. Fibrous and radial Na–Ca sulfates, likely corresponding to hydroglauberite—a common mineral in evaporitic settings—formed more rapidly in the presence of microorganisms (Figs. 6A–B, 7A). The extracellular polymeric substance (EPS) matrix appears to have promoted localized ion accumulation, particularly of Na^+, Ca^{2+}, Mg^{2+}, K^+, and SO_4^{2-}, facilitating nucleation and growth of Na–Ca sulfates and other minerals both within and atop the biofilm (Figs. 8A–B). This mechanism is consistent with previous reports describing EPS-mediated mineralization in microbial mats[63]

[26][2][40][77]. Although gypsum replacement of EPS due to brine evaporation has been documented[3], such effects were minimized in this study by maintaining a constant water level throughout the experiment.

In PAJ, Mg–Si globules were detected exclusively in the presence of microorganisms. These globules, previously identified as protophyllosilicates by Cabestrero et al.[12], occurred within crystal porosities together with allotriomorphic halite embedded in EPS and organic material (Figs. 7D, 8C). The surrounding EPS was enriched in arsenic (Fig. 8D), suggesting selective ion binding within the matrix. Additionally, dumbbell-shaped calcite crystals were observed atop the EPS layer (Fig. 7E). Similar morphologies have been associated with prokaryote-driven biomineralization and the presence of negatively charged functional groups in EPS[78][75].

Lenticular Al–K sulfate aggregates, likely corresponding to alunite, appeared early in GOR (both control and experiment samples) and later in PAJ and LLA (Figs. 7F–G, 8E–F). Pueyo et al.[16] reported alunite as common in GOR, attributing its occurrence to hydrothermal input. The acidic pH of GOR brines and the high availability of Al ions may also favor alunite precipitation. Given that aluminum may be more concentrated in EPS than in the aqueous phase, its association with the biofilm could explain the preferential formation of alunite near microbial colonies. Although filtered brine was used, the early occurrence of alunite might also be related to mineral nucleation during the autoclaving process at 121 °C. Nevertheless, the spatial association between alunite crystals and coccoid cells along gypsum fractures in GOR (Fig. 5I) suggests a possible interaction between them.

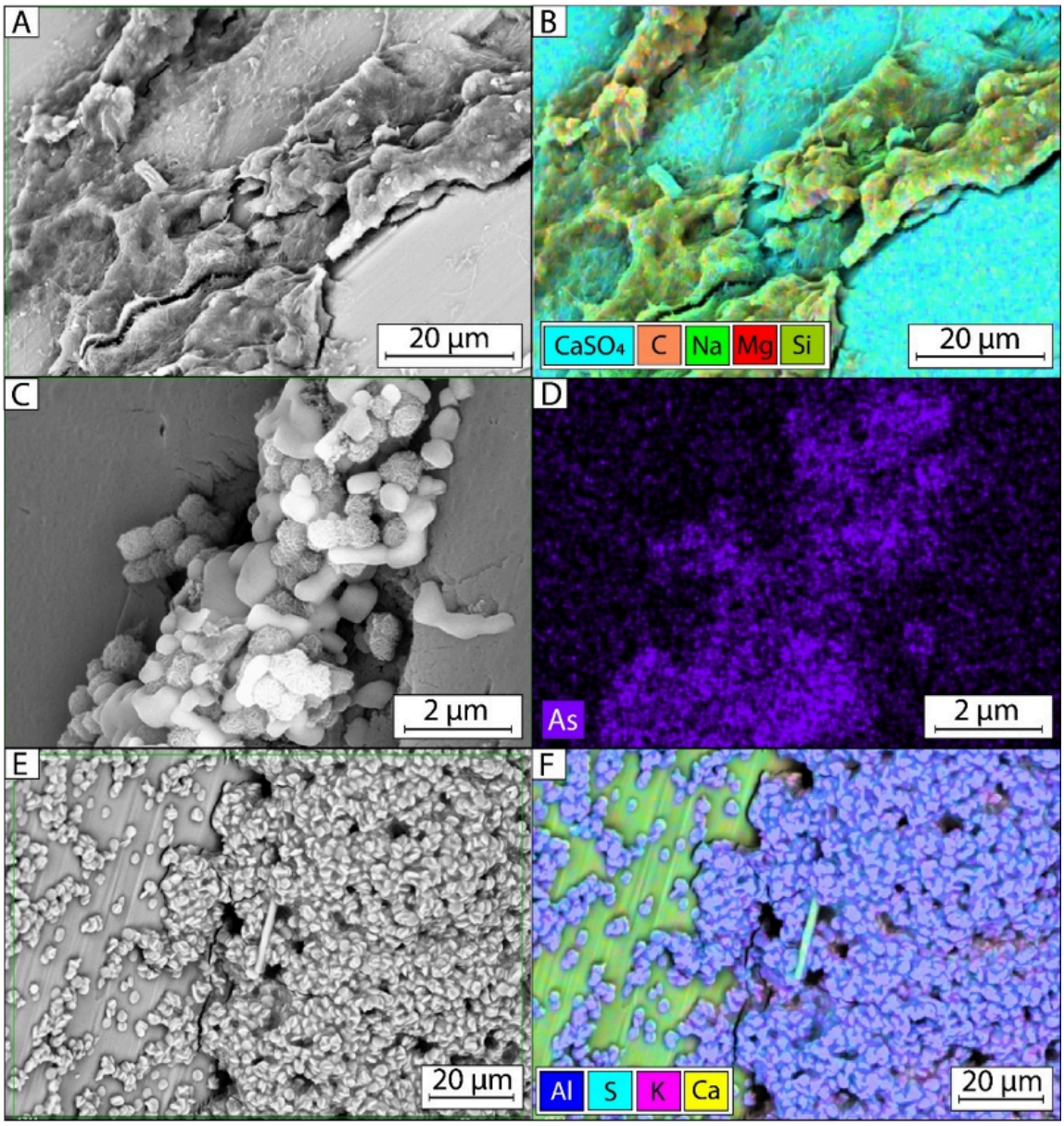

Figure 8. SEM microphotographs (A, C, E) and EDS mapping (B, D, F) of LLA (A-B), PAJ (C-D) and GOR (E-F) gypsum samples. (A) EPS-embedded crystals and cells on gypsum surface. (B) Mg-Si and Na are concentrated below the biomass, suggesting both Mg-Si globules and Na-Ca sulfates are agglutinated. (C) Porosity filled with allotriomorphic halite and Mg-Si globules. (D) Globules appear to be also As-rich according to EDS mapping. (E) Twinned lenticular aggregates covering GOR gypsum surface. (F) EDS mapping shows that they are rich in K, Al and S, suggesting alunite.

doi.org/10.32388/ED4EYH

5. Conclusions

This study demonstrates that microbial activity exerts a measurable influence on gypsum dissolution and secondary mineral formation under controlled conditions. Compared to abiotic controls, microbial systems exhibited smooth, rounded dissolution cavities and porosity fillings by allotriomorphic halite, Mg–Si globules, and extracellular polymeric substances (EPS), features that were particularly abundant in samples from Salar de Pajonales. The results also show that when EPS develops faster than abiotic dissolution, it can act as a protective barrier against further gypsum degradation, as observed in Llamara and Pajonales samples.

Microbially induced mineralization was evidenced by the precipitation of calcite (Pajonales), hydroglauberite (Llamara), and Mg–Si globules with distinctive morphologies and arrangements, pointing to biologically mediated control over nucleation and growth. The contrasting evolution of minerals and microbial communities among the three sites reflects their environmental origins: the circumneutral pH of Llamara and Pajonales supports similar processes, while the highly acidic conditions in Gorbea likely limit microbial growth and alter mineral pathways.

By using natural brines and intact microbial mats under regulated UV/PAR radiation, temperature, and water level, this experiment highlights how microbial consortia can drive mineral diversity, texture, and organization even in the absence of evaporation. The microscopic mineral textures produced over short timescales suggest that longer-term studies are needed to better quantify microbial roles in evaporite evolution.

Finally, this experimental framework—building upon Cabestrero et al.[12]—offers a valuable approach for exploring geomicrobiological processes in hypersaline systems. While focusing on EPS-producing consortia allows the capture of community-level effects, future work should address the specific contributions of individual microbial taxa. The mineral textures observed here may also serve as analogs for biosignature identification in both terrestrial and extraterrestrial evaporitic environments.

Statements and Declarations

Funding

Proyecto CONICYT Postdoctorado 3190821, ANID National Doctoral Scholarship (No. 21181422) and Centro de Biotecnología Alberto Ruiz CBAR-UCN.

Author contributions

C. T.-C., O. C. and C. D., designed and carried out the sampling campaigns at Salar de Llamara, Salar de Pajonales and Salar de Gorbea. O. C., C. T.-C. and I. O. designed the experimental setup with supervision of C. D., and I. O. executed the experiment under supervision from O.C. and C. T.-C. CLSM and fluorescence imaging was carried out by I. O. and C. T.- C., and processed by I. O. Hidrogeochemical modelling and gypsum crystal obtention was performed by I. O. with supervision of O. C. Sampling for SEM-EDS analyses was performed by I. O., and sample preparation was carried out by I. O. and O. C. SEM-EDS analyses were performed at MAINI under supervision from O. C., C. T.-C. and I. O. Data discussion was coordinated by I. O. with aid from O. C, C. T.-C. and C.D. Manuscript was written by I. O., with contributions from all authors.

Acknowledgments

The authors are appreciative of the support from the staff at MAINI and CBAR laboratory facilities, Universidad Católica del Norte, Antofagasta, Chile.

References

1. a, b, c*Dong H, Rech JA, Jiang H, Sun H, Buck BJ (2007). "Endolithic Cyanobacteria in Soil Gypsum: Occurrences in A tacama (Chile), Mojave (United States), and Al-Jafr Basin (Jordan) Deserts." J Geophys Res Biogeosci.* ***112****(G2).*
2. a, b, c, d*Vogel MB, Des Marais DJ, Turk KA, Parenteau MN, Jahnke LL, Kubo MD (2009). "The Role of Biofilms in th e Sedimentology of Actively Forming Gypsum Deposits at Guerrero Negro, Mexico." Astrobiology.* ***9****(9):875–893.*
3. a, b*Rouchy JM, Monty C (2000). "Gypsum Microbial Sediments: Neogene and Modern Examples." In: Microbial S ediments. Berlin, Heidelberg: Springer Berlin Heidelberg. p. 209–216.*
4. a, b, c*Van Driessche AE, Stawski TM, Kellermeier M (2019). "Calcium Sulfate Precipitation Pathways in Natural an d Engineered Environments." Chem Geol.* ***530****:119274.*
5. a, b, c, d*Chong Díaz G, Demergasso C, Urrutia Meza J, Vargas M (2020). "El Dominio Salino del Norte de Chile y Su s Yacimientos de Minerales Industriales" [The Saline Domain of Northern Chile and Its Industrial Mineral Deposi ts]. Bol Soc Geol Mex [Bulletin of the Geological Society of Mexico].* ***72****(3).*
6. a, b, c, d*Reid RP, Oehlert AM, Suosaari EP, Demergasso C, Chong G, Escudero LV, et al. (2021). "Electrical Conductivi ty as a Driver of Biological and Geological Spatial Heterogeneity in the Puquios, Salar de Llamara, Atacama Dese rt, Chile." Sci Rep.* ***11****(1):12769.*
7. a, b*Garcés I, López PL, Auqué LF, Chong G, Valles V, Gimeno MJ (1996). "Características Geoquímicas Generales del Sistema Salino del Salar de Llamara (Chile)" [General Geochemical Characteristics of the Saline System of Salar de Llamara (Chile)]. Estud Geol [Geological Studies].* ***52****(1-2):23–35.*

8. ^*Sáez A (1995). Cenozoic and Quaternary Lacustrine Systems in Northern Chile (Central Andes, Arc and Fore-Arc). Antofagasta: Excursion Guidebook, Recent and Ancient Lacustrine Systems in Convergent Margins. GLO-PALS -International Association of Sedimentalogists Meeting. 77 p.*
9. ^*Sáez A, Cabrera L, Jensen A, Chong G (1999). "Late Neogene Lacustrine Record and Palaeogeography in the Quil lagua–Llamara Basin, Central Andean Fore-Arc (Northern Chile)." Palaeogeogr Palaeoclimatol Palaeoecol. **151**(1 -3):5–37.*
10. ^*Kiefer E, Dorr MJ, Ibbeken H, Gotze HJ (1997). "Gravity-Based Mass Balance of an Alluvial Fan Giant: The Arcas Fan, Pampa del Tamarugal, Northern Chile." Andean Geol. **24**(2):165–185.*
11. a, b, c*Demergasso C, Chong G, Galleguillos P, Escudero L, Martínez-Alonso M, Esteve I (2003). "Tapetes Microbian os del Salar de Llamará, Norte de Chile" [Microbial Mats of Salar de Llamará, Northern Chile]. Rev Chil Hist Nat [Chilean Journal of Natural History]. **76**(3):485–499.*
12. a, b, c, d, e, f, g, h, i, j, k, l*Cabestrero Ó, Tebes-Cayo C, Hinman NW, Demergasso C (2022). "Mineral Paragenesis Preci pitating in Salt Flat Pools of Continental Environments Replicated in Microbial Mat Microcosms Without Evapor ation." Minerals. **12**(5):646.*
13. ^*Chong G, Pereira M, Gonzalez G, Wilke HG (1991). "Los Fenomenos de Remocion en Masa Ocurridos en la Regio n de Antofagasta en Junio de 1991." Rev Fac Ing Cienc Geol. **7**:6–13.*
14. ^*Naranjo JA, Villa V, Venegas C (2013). "Geología de Las Áreas Salar de Pajonales y Cerro Moño, Regiones de Anto fagasta y Atacama" [Geology of the Salar de Pajonales and Cerro Moño Areas, Antofagasta and Atacama Region s]. Santiago: Servicio Nacional de Geología y Minería, Carta Geológica de Chile, Serie Geología Básica 153-154, 1 mapa escala 1:100.000.*
15. ^*Risacher F, Alonso H, Salazar Méndez C (1999). "Geoquímica de Aguas en Cuencas Cerradas: I, II, III Regiones-C hile" [Water Geochemistry in Closed Basins: I, II, III Regions-Chile].*
16. a, b, c*Pueyo Mur JJ, Demergasso C, Escudero L, Chong G, Corttéz-Rivera P, Sanjurjo-Sánchez J, et al. (2021). "On the Origin of Saline Compounds in Acidic Salt Flats (Central Andean Altiplano)." Chem Geol. **574**:120155.*
17. ^*Niemeyer Hans F (1980). Hoyas Hidrográficas de Chile, Segunda Región [Hydrographic Basins of Chile, Second Region]. Santiago de Chile: Ministerio de Obras Públicas (Chile), Dirección General de Aguas.*
18. a, b*Escudero LV, Bijman J, Chong G, et al. (2013). "Geochemistry and Microbiology in an Acidic, High Altitude (4,0 00 M) Salt Flat—High Andes, Northern Chile." Adv Mater Res. **825**:28–32.*
19. a, b*Kemper WD, Olsen J, De Mooy CJ (1975). "Dissolution Rate of Gypsum in Flowing Water." Soil Sci Soc Am J. **39** (3):458–463.*
20. ^*López PL, Auqué LF, Garcés I, Chong G (1999). "Características Geoquímicas y Pautas de Evolución de Las Salmu eras Superficiales del Salar de Llamará, Chile" [Geochemical Characteristics and Evolution Patterns of Surface Br*

*ines of Salar de Llamará, Chile]. Rev Geol Chile [Geological Journal of Chile]. **26**(1):89–108.*

21. ^*Freyer D, Voigt W (2003). "Crystallization and Phase Stability of CaSO4 and CaSO4–Based Salts." Monatsh Che m Chem Monthly [Chemical Monthly]. **134**(5):693–719.*
22. ^*Lebedev AL (2015). "Kinetics of Gypsum Dissolution in Water." Geochem Int. **53**(9):811–824.*
23. ^*Jin Q, Perry LN, Bullard JW (2020). "Temperature Dependence of Gypsum Dissolution Rates." Cem Concr Res. **12 9**:105969.*
24. ^*Otálora F, Criado-Reyes J, Baselga M, Canals A, Verdugo-Escamilla C, García Ruiz JM (2020). "Hydrochemical a nd Mineralogical Evolution Through Evaporitic Processes in Salar de Llamara Brines (Atacama, Chile)." ACS Ear th Space Chem. **4**(6):882–896.*
25. ^*Getenet M, García-Ruiz JM, Otálora F, Emmerling F, Al-Sabbagh D, Verdugo-Escamilla C (2022). "A Comprehensi ve Methodology for Monitoring Evaporitic Mineral Precipitation and Hydrochemical Evolution of Saline Lakes: The Case of Lake Magadi Soda Brine (East African Rift Valley, Kenya)." Cryst Growth Des. **22**(4):2307–2317.*
26. a, b, c*Dupraz C, Reid RP, Braissant O, Decho AW, Norman RS, Visscher PT (2009). "Processes of Carbonate Precipit ation in Modern Microbial Mats." Earth-Sci Rev. **96**(3):141–162.*
27. ^*Rickard D (2012). Sulfidic Sediments and Sedimentary Rocks. Vol. 65. Newnes.*
28. ^*Farias ME, Contreras M, Rasuk MC, Kurth D, Flores MR, Poire DG, et al. (2014). "Characterization of Bacterial Di versity Associated With Microbial Mats, Gypsum Evaporites and Carbonate Microbialites in Thalassic Wetlands: Tebenquiche and La Brava, Salar de Atacama, Chile." Extremophiles. **18**(2):311–329.*
29. ^*Chen S, Watkins JM (2025). "Oxygen and Carbon Isotopes in Marine Carbonates: A Biogenic Climate Archive Bu ilt Upon Disequilibria." Elements. **21**(2):112–117.*
30. ^*Daëron M, Drysdale RN, Peral M, Huyghe D, Blamart D, Coplen TB, et al. (2019). "Most Earth-Surface Calcites Pr ecipitate Out of Isotopic Equilibrium." Nat Commun. **10**(1):429.*
31. a, b*Reid RP, Visscher PT, Decho AW, Stolz JF, Bebout BM, Dupraz C, et al. (2000). "The Role of Microbes in Accretio n, Lamination and Early Lithification of Modern Marine Stromatolites." Nature. **406**(6799):989–992.*
32. a, b*Cody AM, Cody RD (1991). "Chiral Habit Modifications of Gypsum From Epitaxial-Like Adsorption of Stereosp ecific Growth Inhibitors." J Cryst Growth. **113**(3-4):508–519.*
33. a, b*Dupraz C, Visscher PT (2005). "Microbial Lithification in Marine Stromatolites and Hypersaline Mats." Trends Microbiol. **13**(9):429–438.*
34. ^*Dupraz C, Visscher PT, Baumgartner LK, Reid RP (2004). "Microbe–Mineral Interactions: Early Carbonate Preci pitation in a Hypersaline Lake (Eleuthera Island, Bahamas)." Sedimentology. **51**(4):745–765.*
35. a, b*Glunk C, Dupraz C, Braissant O, Gallagher KL, Verrecchia EP, Visscher PT (2011). "Microbially Mediated Carbon ate Precipitation in a Hypersaline Lake, Big Pond (Eleuthera, Bahamas)." Sedimentology. **58**(3):720–736.*

36. ^Konhauser KO (2007). Introduction to Geomicrobiology. Oxford, UK: Blackwell Publishing. p. 146.

37. a, b, cThompson JB, Ferris FG (1990). "Cyanobacterial Precipitation of Gypsum, Calcite, and Magnesite From Natu ral Alkaline Lake Water." Geology. **18**(10):995–998.

38. ^Harouaka K, Mansor M, Macalady JL, Fantle MS (2016). "Calcium Isotopic Fractionation in Microbially Mediate d Gypsum Precipitates." Geochim Cosmochim Acta. **184**:114–131.

39. ^Sánchez-Román M, Vasconcelos C, Warthmann R, Rivadeneyra M, McKenzie JA (2009). "Microbial Dolomite Pr ecipitation Under Aerobic Conditions: Results From Brejo do Espinho Lagoon (Brazil) and Culture Experiments." Perspectives in Carbonate Geology: A Tribute to the Career of Robert Nathan Ginsburg. p. 167–178.

40. a, b, cSanz-Montero ME, Cabestrero Ó, Sánchez-Román M (2019). "Microbial Mg-Rich Carbonates in an Extreme Alkaline Lake (Las Eras, Central Spain)." Front Microbiol. **10**:148.

41. ^Tourney J, Ngwenya BT (2009). "Bacterial Extracellular Polymeric Substances (EPS) Mediate CaCO3 Morpholo gy and Polymorphism." Chem Geol. **262**(3-4):138–146.

42. ^Tourney J, Ngwenya BT (2014). "The Role of Bacterial Extracellular Polymeric Substances in Geomicrobiology." Chem Geol. **386**:115–132.

43. ^Jarwar MA, Dumontet S, Pasquale V, Chen C (2022). "Microbial Induced Carbonate Precipitation: Environments, Applications, and Mechanisms." Geomicrobiol J. **39**(10):833–851.

44. ^Friedmann EI (1980). "Endolithic Microbial Life in Hot and Cold Deserts." Origins Life. **10**(3):223–235.

45. ^Friedmann EI, Kibler AP (1980). "Nitrogen Economy of Endolithic Microbial Communities in Hot and Cold Dese rts." Microb Ecol. **6**(2):95–108.

46. a, bCámara B, Souza-Egipsy V, Ascaso C, Artieda O, De Los Ríos A, Wierzchos J (2016). "Biosignatures and Microbi al Fossils in Endolithic Microbial Communities Colonizing Ca-Sulfate Crusts in the Atacama Desert." Chem Geol. **443**:22–31.

47. ^Meslier V, Casero MC, Dailey M, Wierzchos J, Ascaso C, Artieda O, et al. (2018). "Fundamental Drivers for Endolit hic Microbial Community Assemblies in the Hyperarid Atacama Desert." Environ Microbiol. **20**(5):1765–1781.

48. a, bWierzchos J, Casero MC, Artieda O, Ascaso C (2018). "Endolithic Microbial Habitats as Refuges for Life in Polye xtreme Environment of the Atacama Desert." Curr Opin Microbiol. **43**:124–131.

49. a, bWierzchos J, Ascaso C, Artieda O, Casero MC (2020). "The Desert Polyextreme Environment and Endolithic Ha bitats." In: Microbial Ecosystems in Central Andes Extreme Environments: Biofilms, Microbial Mats, Microbialites and Endoevaporites. Cham: Springer International Publishing. p. 37–49.

50. ^Sajjad W, Ilahi N, Kang S, Bahadur A, Zada S, Iqbal A (2022). "Endolithic Microbes of Rocks, Their Community, F unction and Survival Strategies." Int Biodeterior Biodegrad. **169**:105387.

51. ^a, b, cWierzchos J, DiRuggiero J, Vítek P, Artieda O, Souza-Egipsy V, Škaloud P, et al. (2015). "Adaptation Strategies of Endolithic Chlorophototrophs to Survive the Hyperarid and Extreme Solar Radiation Environment of the Atacama Desert." Front Microbiol. **6**:934.

52. ^a, bRoldán M, Ascaso C, Wierzchos J (2014). "Fluorescent Fingerprints of Endolithic Phototrophic Cyanobacteria Living Within Halite Rocks in the Atacama Desert." Appl Environ Microbiol. **80**(10):2998–3006.

53. ^Liu ST, Nancollas GH (1973). "The Crystal Growth of Calcium Sulfate Dihydrate in the Presence of Additives." J Colloid Interface Sci. **44**(3):422–429.

54. ^Witkamp GJ, Van der Eerden JP, Van Rosmalen GM (1990). "Growth of Gypsum: I. Kinetics." J Cryst Growth. **102**(1-2):281–289.

55. ^Parkhurst DL, Appelo CAJ (2013). Description of Input and Examples for PHREEQC Version 3—A Computer Program for Speciation, Batch-Reaction, One-Dimensional Transport, and Inverse Geochemical Calculations. US Geological Survey Techniques and Methods. **6**(A43):497.

56. ^Díaz C, Maidana N (2005). Diatomeas de Los Salares Atacama y Punta Negra, II Región, Chile. Santiago, Chile: Centro de Ecología Aplicada Ltda.

57. ^Tebes C, Rodriguez C, Demergasso C, Chong G, Hinman N, Parro V (2019). "Microbial Participation on the Production and Preservation of Gypsum Structures From Salar de Pajonales, Northern of Chile." Geophys Res Abstr. **21**.

58. ^a, bEscudero L, Oetiker N, Gallardo K, Tebes-Cayo C, Guajardo M, Nuñez C, et al. (2018). "A Thiotrophic Microbial Community in an Acidic Brine Lake in Northern Chile." Antonie Van Leeuwenhoek. **111**(8):1403–1419.

59. ^Salazar-Ardiles C, Asserella-Rebollo L, Andrade DC (2022). "Free-Living Amoebas in Extreme Environments: The True Survival in Our Planet." BioMed Res Int. **2022**(1):2359883.

60. ^a, bVenturi S, Crognale S, Di Benedetto F, Montegrossi G, Casentini B, Amalfitano S, et al. (2022). "Interplay Between Abiotic and Microbial Biofilm-Mediated Processes for Travertine Formation: Insights From a Thermal Spring (Piscine Carletti, Viterbo, Italy)." Geobiology. **20**(6):837–856.

61. ^Jehlička J, Oren A, Vítek P, Wierzchos J (2024). "Microbial Colonization of Gypsum: From the Fossil Record to the Present Day." Front Microbiol. **15**:1397437.

62. ^a, bRothschild LJ, Giver LJ, White MR, Mancinelli RL (1994). "Metabolic Activity of Microorganisms in Evaporites 1." J Phycol. **30**(3):431–438.

63. ^a, bSanz-Montero ME, Rodríguez-Aranda JP, Calvo JP (2006). "Mediation of Endoevaporitic Microbial Communities in Early Replacement of Gypsum by Dolomite: A Case Study From Miocene Lake Deposits of the Madrid Basin, Spain." J Sediment Res. **76**(12):1257–1266.

64. ^Rios-Valenciana EE, Briones-Gallardo R, Chazaro-Ruiz LF, Lopez-Lozano NE, Sierra-Alvarez R, Celis LB (2020). "Dissolution and Final Fate of Arsenic Associated With Gypsum, Calcite, and Ferrihydrite: Influence of Microbial

Reduction of As (V), Sulfate, and Fe (III)." Chemosphere. ***239****:124823.*

65. ^*Ostroff AG, Metler AV (1966). "Solubility of Calcium Sulfate Dihydrate in the System NaCl-MgCl2-H2O From 28° to 70° C." J Chem Eng Data.* ***11****(3):346–350.*
66. ^*Reyes JC, Muñoz FO, Ruiz JMG (2017). "Pautas de Disolución de Estromatolitos de Yeso en el Desierto de Atacam a." Macla: Rev Soc Española Mineral.* ***22****:33–34.*
67. ^*Rasuk MC, Kurth D, Flores MR, Contreras M, Novoa F, Poire D, Farias ME (2014). "Microbial Characterization of Microbial Ecosystems Associated to Evaporites Domes of Gypsum in Salar de Llamara in Atacama Desert." Micro b Ecol.* ***68****(3):483–494.*
68. ^*Tebes-Cayo C, Demergasso C, Chong G, Cabestrero Aranda Ó, Sanz Montero ME, Castro-Nallar E, Cabrol N (202 1). "Geoquímica y Comunidades Microbianas en Los Salares de Pajonales y de Gorbea (Chile): Influencia en La Fo rmación de Microbialitos de Yeso" [Geochemistry and Microbial Communities in the Pajonales and Gorbea Salt Flats (Chile): Influence on the Formation of Gypsum Microbialites].*
69. ^*Tebes-Cayo C, Demergasso C, Chong G, Cabestrero Aranda Ó, Sanz Montero ME, Castro-Nallar E, Cabrol N (202 1). "Geoquímica y Comunidades Microbianas en Los Salares de Pajonales y de Gorbea (Chile): Influencia en La Fo rmación de Microbialitos de Yeso." Geoquímica y Comunidades Microbianas en Los Salares de Pajonales y de Go rbea (Chile): Influencia en La Formación de Microbialitos de Yeso.*
70. ^*Osman JR, Wang Y, Jaubert C, Nguyen TN, Fernandes GR, DuBow MS (2021). "The Bacterial Communities of Sur face Soils From Desert Sites in the Eastern Utah (USA) Portion of the Colorado Plateau." Microbiol Res.* ***244****:12666 4.*
71. ^*Rossi F, De Philippis R (2015). "Role of Cyanobacterial Exopolysaccharides in Phototrophic Biofilms and in Com plex Microbial Mats." Life.* ***5****(2):1218–1238.*
72. ^*Laroche C (2022). "Exopolysaccharides From Microalgae and Cyanobacteria: Diversity of Strains, Production St rategies, and Applications." Mar Drugs.* ***20****(5):336.*
73. ^*Davis-Belmar CS, Pinto E, Demergasso C, Rautenbach G (2013). "Proteo and Actinobacteria Diversity at a Sulfid e, Salt and Acid-Rich Lake in the North of Chile." Adv Mater Res.* ***825****:37–41.*
74. a, b*DiRuggiero J, Wierzchos J, Robinson CK, Souterre T, Ravel J, Artieda O, et al. (2013). "Microbial Colonisation of Chasmoendolithic Habitats in the Hyper-Arid Zone of the Atacama Desert." Biogeosciences.* ***10****(4):2439–2450.*
75. a, b*Zhang Y, Yang J, Cao X (2020). "Effects of Several Retarders on Setting Time and Strength of Building Gypsu m." Constr Build Mater.* ***240****:117927.*
76. ^*Cody RD, Cody AM (1988). "Gypsum Nucleation and Crystal Morphology in Analog Saline Terrestrial Environm ents." J Sediment Res.* ***58****(2):247–255.*

77. ^del Buey P, Sanz-Montero ME, Braissant O, Cabestrero Ó, Visscher PT (2021). "The Role of Microbial Extracellular Polymeric Substances on Formation of Sulfate Minerals and Fibrous Mg-Clays." Chem Geol. **581**:120403.

78. ^Lv JJ, Ma F, Li FC, Zhang CH, Chen JN (2017). "Vaterite Induced by Lysinibacillus Sp. GW-2 Strain and Its Stability." J Struct Biol. **200**(1):97–105.

Declarations

Funding: Proyecto CONICYT Postdoctorado 3190821, ANID National Doctoral Scholarship (No. 21181422) and Centro de Biotecnología Alberto Ruiz CBAR-UCN.

Potential competing interests: No potential competing interests to declare.